

Figure 6.4. Electric resistance variation of the piezoresistive composites (with the maximum filler amount) as a function of the applied uniaxial pressure.

all the processability problems (mixing and curing).

The copper and nickel based composite have comparable responses in the range up to 2 MPa (in particular at low pressure values) with a maximum variation of electrical resistance of nine orders of magnitude for the PDMS-Ni (seven for PDMS-Cu). Instead the gold based composite exhibits a variation of five orders and is less sensible to small pressure values. Nickel and copper are then more suited for application with an elevate sensitivity and a wide range of measurement.

6.3 Conclusion

Summarizing the analysis on the minimum and on the maximum amount of filler in the piezoresistive composite one can note that each metal particle has its advantages and disadvantages. We have experimentally observed a strong dependence of the filler amount from the morphological figures of merit. We have found out that particles with sharp tip and small core size, i.e., high H_t/D_{core} and $H_t/FWHM$, together with a small curvature radius of the tip (R_t), present strong enhancement of the tunnelling conduction.

Gold particles were synthesized and *ad-hoc* prepared, whereas both Cu and Ni particles

were obtained commercially. This allows a full control on the size and shape of the gold nanostars with a very good reproducibility, which cannot be reached with the other two metals. Moreover its nanometric size and tip nanostructuring allow the use of gold fillers in small amounts in the composite, thus obtaining comparable piezoresistive performances than the other composites with commercial fillers. Furthermore, gold shows higher resistance to oxidation with respect to both nickel and copper and is a safe material (whereas nickel particles were reported to be carcinogenic, because of oxidation in air). In addition, thanks to the small content of the filler required and its nanometric size, the gold nanostars can be used to prepare very flexible, light, and thin composites, ideal for the integration in MEMS-like technology for tactile sensor applications. The drawbacks are the time required for the synthesis process, the low synthesis yield which, combined with a difficult scalability, makes challenging the production of grams of nanoparticles, the problems in processing and curing the composite with metal content above 100 phr, and above all the elevated cost of the starting chemical precursors.

Nickel based composites have a very high sensitivity and they are easy to process. Both the minimum and maximum amounts of filler necessary to have piezoresistive responses comparable with the other metal based composites are higher than the gold and copper quantities, but it is not a big drawback since the cost of the powder is negligible with respect to the polymeric matrix one (it is produced and sold in tons amount for different application in metallurgy, chemistry and electronics). The main disadvantages are the oxidation of the surface of the particles, that can cause a degradation of the functional response of the composite, and the safety problem. In fact nickel oxide is suspected of carcinogenic effect for inhalation, so even if we worked with the nickel particles (not directly with the oxide) and they are integrated in the polymer matrix, we moved to prepared the composite with copper particles as filler.

Finally, copper presents advantages and disadvantages comparable with the nickel ones except for the safety problems. Moreover the minimum and maximum filler amounts are lower than the nickel ones, even if the cost of the powder is very low for its elevated utilization in sintering and chemical application. For these reasons the PDMS-Cu composites substituted the PDMS-Ni ones in the development of the second generation of matrix tactile sensor and in the fabrication of the pressure sensor based on resonant frequency shifting, as it will be shown in the following chapters.

Bibliography

- [1] R. Strumpler and J. Glatz-Reichenbach. Conducting polymer composites. *Journal of Electroceramics*, 3(4):329–346, 1999.
- [2] S.Y. Fu, X.Q. Feng, B. Lauke, and Y.W. Mai. Effects of particle size, particle/matrix interface adhesion and particle loading on mechanical properties of particulate-polymer composites. *Composites Part B: Engineering*, 39(6):933–961, 2008.
- [3] D. Bloor, K. Donnelly, P. J Hands, P. Laughlin, and D. Lussey. A metal-polymer composite with unusual properties. *J. Phys. D: Appl. Phys.*, 38:2851–2860, 2005.
- [4] G. Canavese, M. Lombardi, S. Stassi, and C. F. Pirri. Comprehensive characterization of large piezoresistive variation of Ni-PDMS composites. *Applied Mechanics and Materials*, 110-116:1336–1344, 2012.
- [5] M.K. Abyaneh and S.K. Kulkarni. Giant piezoresistive response in zinc-polydimethylsiloxane composites under uniaxial pressure. *J. Phys. D: Appl. Phys.*, 41:135405, 2008.
- [6] C.J. Edgcombe and U. Valdrè. Microscopy and computational modelling to elucidate the enhancement factor for field electron emitters. *Journal of Microscopy*, 203:188–194, 2001.

Chapter 7

Fabrication of a flexible piezoresistive matrix tactile sensor for humanoid robot

The construction of tactile sensing devices, offering the sensitivity and precision in manipulation of objects, is a key focus in research fields concerning industrial automation, service robots, and in particular space human robotics. Distributed tactile sensors are essential for humanoid and space service robot to obtain dynamic whole-body motion control [1, 2]. The necessary requirements should include: (i) the complete coverage of the robot surface in order to detect collision when operating in unstructured environments, (ii) the high resolution and precision for the machine interaction with the external environment, and (iii) the dexterous object manipulation [3, 4].

Composite polymeric materials with piezoresistive properties are one of the best candidates to fabricate a sensing “skin” able to reproduce the tactile sense and to fit the shape of the robot structure. Beyond the high conformability, these sensing materials have usually a wide range of sensitivity, a low power consumption and an elevated mechanical resistance, protecting the system from overpressure, shock and vibrations [5].

To couple this sensing material to the robot structure, the composite has to be integrated in a sensor device. In order to push the spatial sensor resolution beyond the human tactile sense performance (approximately 1mm [6]) MEMS-like technology needs to be used. Two different sensor matrix architectures could be adopted to produce sensing skin based

on piezoresistive composite: (i) integration of the composite into an array or network of separated devices [7, 8, 9] or (ii) a continuous sensing film [10, 4, 11]. The electronic signal conditioning is often embedded into the actual sensor circuit (multiplexing, voltage/current control and measurement) to simplify the system routing.

Data acquisition and transmission, thus the key aspects of the entire system [12], are performed by microcontrollers and data acquisition units, in “real-time” or “quasi real-time” conditions in order to assure the needed system response fastness to external stimuli. Rigid-flexible media are normally employed: rigid PCB are used for the circuit part devoted to signal conditioning, while flexible ribbon cables are adopted for sensor mounting. The information is then transmitted and remotely post-processed to obtain the required pressure information, by specific algorithms implemented either on DSPs/FPGAs rather than ASIC cards, or even directly on PCs, e.g. by programs like Matlab or *ad-hoc* program [1]. The choice among the different solutions is driven by the system dimensions, number of samples, fast prototyping, and, above all, the cost related issues.

In this chapter we prepared self standing multilayer thin samples from the functional materials presented in the previous chapters. Thanks to the high flexibility and easy conformability, the piezoresistive composite materials were used and tested to fit in complex-shaped structures and to be suitably integrated onto the robot surface for tactile sensing. Two process flows based on microcasting and hot embossing techniques were optimized and studied to promote both the sensor spatial resolution and the pressure sensitivity. The latter solution was chosen, since it is well adapted to cover a large robot surface with a continuous and ergonomic layer. The sensing mechanism enrolls the electric resistance variation of a conductive element upon an applied mechanical stress. The variation of resistance is measured between two working electrodes, across the thickness of the conductive sensing material.

The piezoresistive samples were then prepared to form a matrix of sensing element and connected to a dedicated read-out circuit. The electronic board measures the resistance of 8x8 point with a scan rate of the whole matrix of 20 Hz and the signals are successively converted in pressure values by a software and shown with a graphical interface on the PC screen.

7.1 Processability of the composite

7.1.1 Technological process flows

Two different experimental strategies were exploited for the sensor matrix fabrication. The former is based on a microcasting technique to conform the composite material, while the latter consists of a hot embossing method in which the functional material forms a continuous layer, with a constant thickness, between the patterned electrodes.

Concerning the first approach, three different processes were developed for the master fabrication and they are sketched in Fig.7.1. In particular, a milling technique was used in order to direct machining the desired master shape in PMMA substrate (Fig.7.1(a)). This technique allows to obtain moderate sensor matrix resolution since the dimension of the single cell depends on the milling cutter diameter ($300\ \mu\text{m}$ in this work).

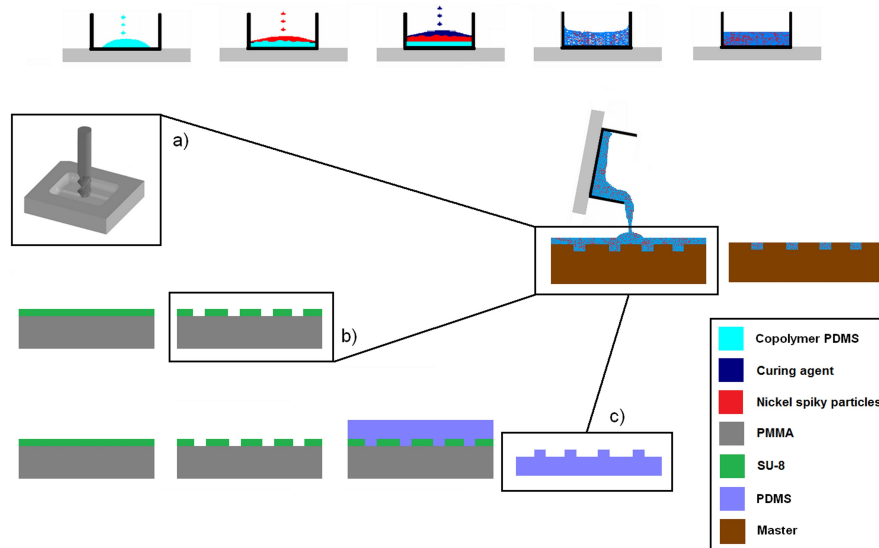


Figure 7.1. Microcasting process flow: Preparation of the piezoresistive composite (first row): PDMS copolymer weighing, Ni particles weighing, curing agent weighing, mixing, mixture outgassing, Three different process flows for the preparation of the micromoulds for piezoresistive composite casting: (a) Micromilling technique, (b) SU-8 lithography: SU-8 spin coating on PMMA substrate, (c) PDMS micromould fabricated by SU-8 master.

The second process flow is based on SU-8 lithography. SU-8 2100 (MicroChem Corp.) negative photoresist was spin coated on a PMMA substrate in order to produce the mould with micrometric controlled size and shape. By varying the spinning rate between 1200 to

2000 rpm, four different thicknesses ($300\mu\text{m}$, $200\mu\text{m}$, $170\mu\text{m}$ and $150\mu\text{m}$) of SU-8 layer were obtained. The process flow is reported in Fig.7.1(b) and more detailed description of the recipe can be found elsewhere [13]. The main drawback of this method is the low durability of the master (less than ten replicas) since SU-8 is fragile and shows low adhesion to the substrate.

The last process flow has been developed to overcome the limits of the previous ones. Instead of using directly the SU-8 master to produce the piezoresistive composite replicas, the SU-8 master was employed to fabricate a second and more resistant soft silicone mould (Fig.7.1(c)). The cured PDMS structure was then surface treated by wetting the mould with a phosphate buffer solution containing the hydrophilic polymer hydroxypolymethylcellulose (HPMC) in order to avoid strong bonding with the composite materials [14] and assure the easy release of composite samples.

Fig.7.2 reports two images of micromould, the first (Fig.7.2(a)) shows a sample produced by milling technique (corresponding to the process flow schematized in Fig.7.1(a)) while the second (Fig.7.2(b)) illustrates a PDMS soft micromould fabricated using the SU-8 rigid master (corresponding to the process flow schematized in Fig.7.1(c)).

Finally the piezoresistive composite was poured in the microfabricated moulds and then

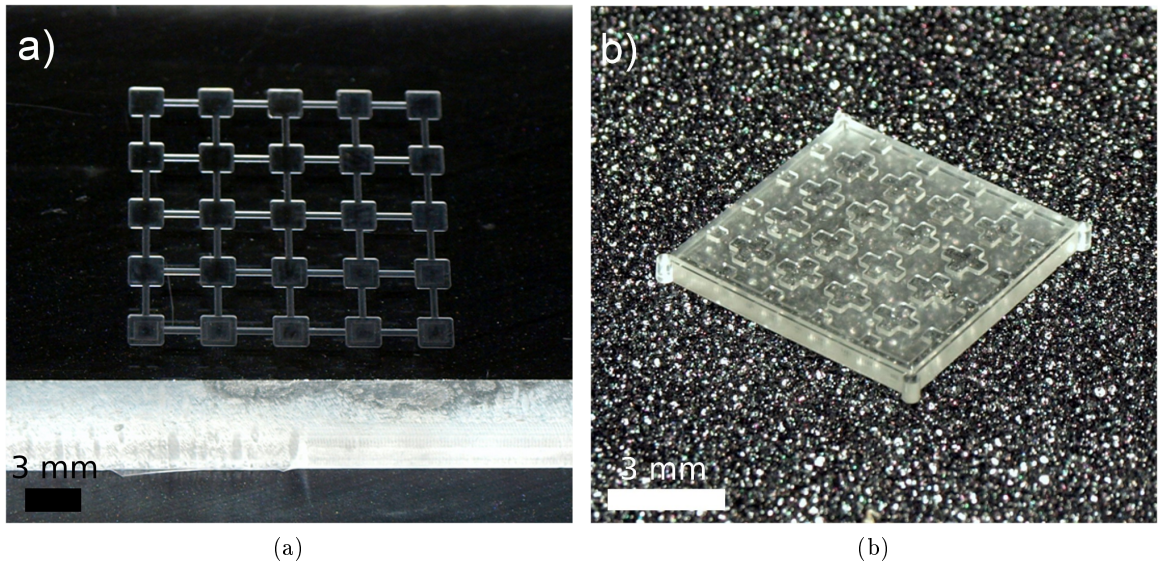


Figure 7.2. (a) PMMA mould fabricated using the micromilling technology, (b) PDMS soft micromould fabricated using the SU-8 rigid master. The scale bar size is 3 mm.

thermally cured in oven at 75°C for three hours.

The process flow of the second experimental strategy is reported in Fig.7.3. In order to mould the composite materials in a controlled form, a PMMA master composed of three separated parts was fabricated by milling technique. Two planar plates were used as rigid top and bottom clamping plates, while a lateral frame was adopted to define the footprint of the sensor. Bottom and top electrodes were made of 50 μm thick metalized polyimide film (Kapton, DuPont). Copper metalized polyimide samples were coated by positive photoresist and then patterned by UV lithography. Furthermore, the metal was selectively etched in Iron (III) chloride in order to use the metal pattern as electrodes. The same lithographic pattern (straight parallel strips) was used to mask both top and bottom electrodes, sandwiching the composite material, that were sealed orthogonally to each other in order to form an electrode matrix. Bottom and top electrodes were clamped between the planar plates respectively below and on the lateral frame. The hybrid structure composed of the piezoresistive composite material embedded in two polyimide films was obtained by pressing and heating the multilayer for three hours at 75°C. The desired composite thickness was obtained by controlling the thickness of the lateral frame mould. Since the composite material and the electrodes layer are cured *in situ*, this approach overcomes the demoulding and the electrode adhesion problems observed with the other microcasting techniques described above. Moreover this process is less expensive and less time consuming with respect to the solutions based on the microcasting strategy.

7.1.2 Material characterization

Thinner composite samples have bigger piezoresistance response, but this behaviour is not linear with the thickness. Thick PDMS-Ni layers were obtained by the microcasting technique from moulds prepared by the micromilling machine, whereas samples with a thickness up to few hundreds of micrometer, were obtained with SU-8 lithography. The piezoresistive response as function of the thickness was evaluated on the samples obtained by both techniques. By means of the milling process, the minimum thickness of the PDMS-Ni layer obtained was 300 μm . The piezoresistive behaviour of this sample compared with the 1 mm thick one is plotted in Fig.7.4(a). Both samples present a similar initial resistance, but under compressive forces the thinner sample experiences a more pronounced variation of the electrical resistance. Further increase in the sensing behaviour was obtained with the layer

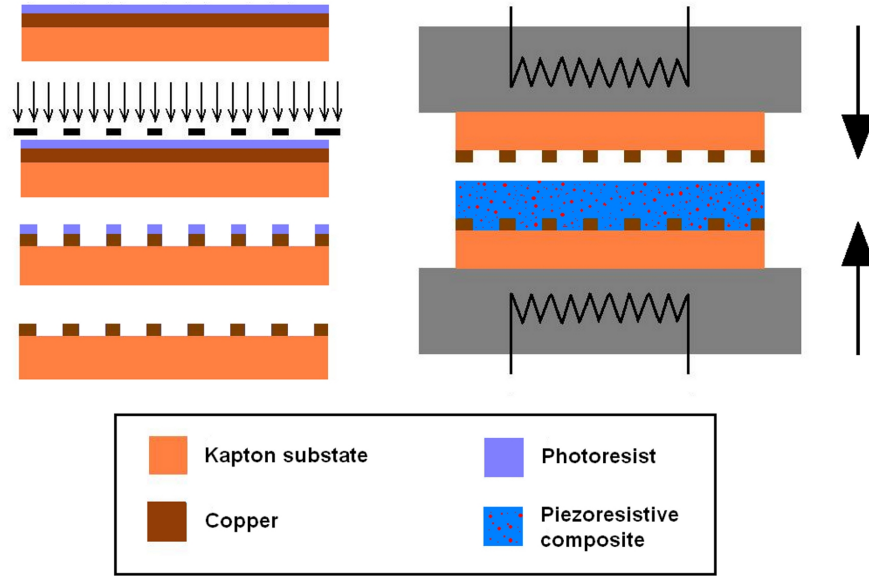


Figure 7.3. Hot embossing process flow: UV lithography on metalized polyimide film, copper etching, hot embossing of the piezoresistive composite between polyimide films.

prepared by the soft lithography process. The $300\ \mu\text{m}$ sample showed a piezosensitivity of about $0.0318/\text{Pa}$, whereas $0.0114/\text{Pa}$ were obtained with the $1\ \text{mm}$ thick sample produced using the milling technique. The obtained pressure sensitivity abundantly overcomes the accepted human skin load sensitivity [15, 16].

Fig.7.4(b) shows the piezoresistive response of 150 , 170 and $200\ \mu\text{m}$ thick samples. In absence of pressure, the value of the electrical resistance measured in these thin samples decreases up to $10\ \text{M}\Omega$ in the $200\ \mu\text{m}$ thick sample and it is even lower in the 170 and $150\ \mu\text{m}$ ones. This phenomenon is probably due to the impossibility, with the sample holder developed in-house, of ensuring the electrical contact without applying a load. Consequently, for what concerns the most sensing and thinnest samples this implies to start the electrical measurement above the undeformed condition.

The PDMS-Ni sensing networks produced using SU-8 master are enough spatially resolved if compared to human skin. In addition they do not present any crosstalk phenomenon between the different cells, because of the empty space between them (that could be filled with insulating polymer) and of the fine width of the connective scrap. These technologies

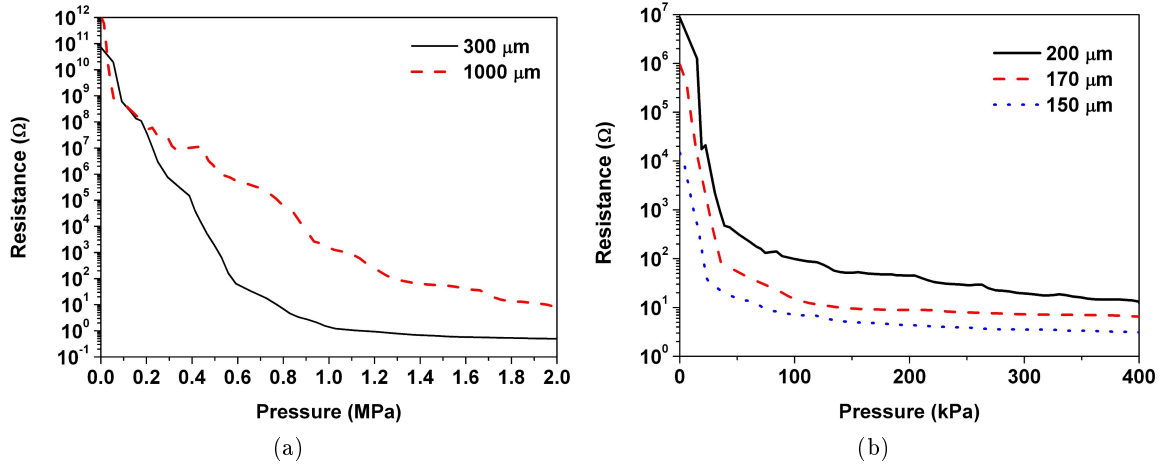


Figure 7.4. Electrical resistance of PDMS-Ni composites as a function of the compressive stress and thickness for: (a) 300 μm and 1 mm thick samples, obtained with milling process and (b) 200, 170 and 150 μm thick samples, prepared by soft lithographic process. The samples were prepared with a nickel-PDMS content of 500 phr and PDMS copolymer-curing agent ratio of 10:1.

require several process steps and an elevate consumption of additional material for the fabrication of a device. Moreover the used pattern is hardly reproducible on larger scale device.

In order to obtained cheaper samples, less time consuming and easiest scalability, a process based on hot-embossing technique was developed. Samples with the same thickness as the ones presented above were prepared with this technique and characterized. The functional results obtained on the composites prepared with the hot-embossing process were similar to the results of the samples produced through microcasting process (same thickness and area). These results confirmed that the piezoresistive properties of the free-standing composite material films are not depending on the technology process, but basically only on the composition (ratio PDMS-Ni) and on the thickness.

On the other hand the potential problem of the hot embossing process is the discretization of the electrical signal, since crosstalk phenomenon can occur if the resistance is measured in two neighboring points of the continuous film. Attenuation measurements were performed in order to understand this effect and thus proceed with the correct design of the electrode pattern, having proper dimension and spacing. A circular metallic disk (2 mm of diameter) was pressed with a pressure of 2 MPa on a continuous layer of PDMS-Ni composite with a fixed thickness. Then the electrical resistance was measured with an equal disk, used as

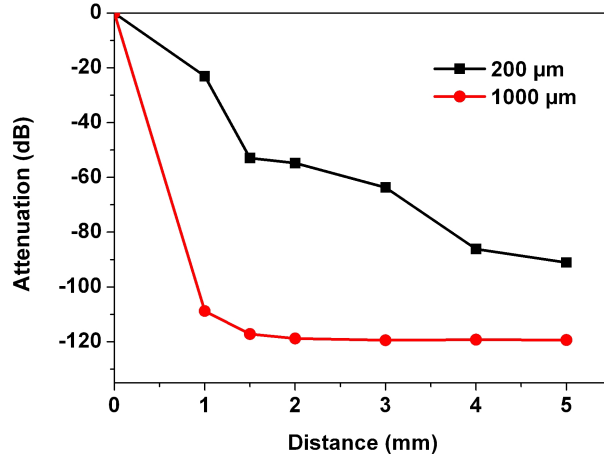


Figure 7.5. Attenuation of the electrical conductance in 200 and 1000 μm thick films at different distances from the compression area.

electrode, at different distances with respect to the pressed area. In Fig.7.5 are plotted the attenuation of the electrical conductance versus the value of the compression point for composite layer 200 and 1000 μm thick. It was found that in 1 mm thick film the attenuation is almost total, even at a distance of 1 mm, whereas in thinner layer the resistance value is decreasing slowly. However for the 200 μm thick film at a distance of 1 mm the attenuation is more than 20 dB, that is a good value for tactile sensor application, and moving to 1.5 mm the attenuation is over 50 dB.

Consequently the electrode pattern was designed considering the attenuation measurements and the desired tactile resolution.

7.2 First generation matrix tactile sensor

7.2.1 Sensor design and readout circuitry

The sensor was prepared by hot embossing techniques with area $40 \times 40 \text{ mm}^2$ and thickness of 1 mm. The 8×8 array pattern was fabricated by designing 8 parallel lines on 2 copper metalized polyimide foil used as bottom and top electrodes. The lines were 2 mm thick and the space among them was 3 mm, in line with the constraints obtained in Section 7.1.2.

The electronic board constantly monitors the sensing material and sends the acquired data to a PC that processes them in real-time, thus providing the instantaneous intensity and spatial distribution of the pressure. The architecture of the overall system and an image

of sensor matrix attached to the electronic board are reported in Fig.7.6.

The membrane can be modeled as a two-dimensional array of resistors whose value decreases by increasing the applied pressure. Therefore, resistance measurements performed on each resistor of the matrix can indirectly provide both the pressure intensity and the pressure distribution.

In the proposed system, the measure of each resistor is performed by fixing a known voltage across the selected element and by measuring the current that consequently flows through it. Two analog multiplexers, one for the row and one for the column respectively, are employed to scan all the elements of the matrix and connect one resistor at time to the measuring circuit through a low impedance path, while leaving all the others paths at high impedance. The multiplexers have to be carefully chosen to ensure that their leakage current remains negligible with respect to the minimum current expected when no pressure is applied on the sensing material. Then the current flows in a current-voltage converter.

The characterization of the material showed that the resistance of the membrane, and therefore also the flowing current, can span over several decades depending on the applied pressure. A typical membrane can exhibits a variation of resistance between 10^2 to $10^7 \Omega$, therefore, choosing a voltage of 1 V, the current will result in the range 100 nA - 10 mA.

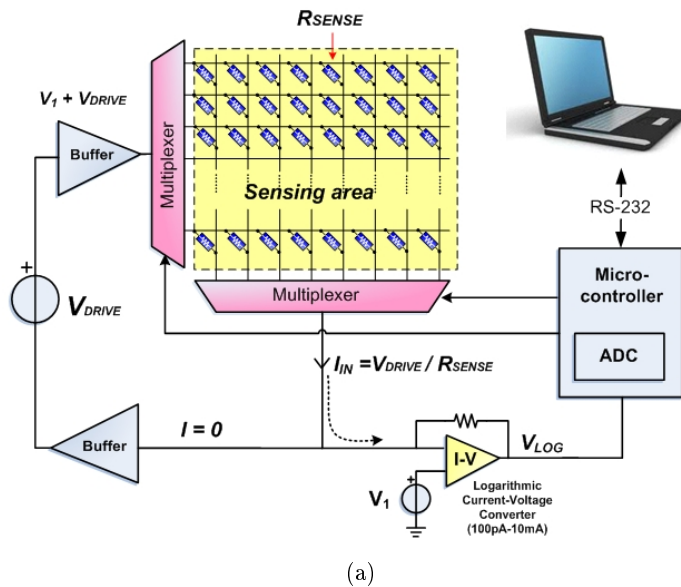


Figure 7.6. (a) Schematic and (b) image of the overall system.

Moreover choosing 1 V as operation voltage one can avoid the charging effect and inversion of the current slope observed in the I-V characteristics (presented in Section 3.7).

To tackle this huge range, a logarithmic trans-impedance amplifier was selected. This device allows the conversion of current from 100 pA to 10 mA, which corresponds to a span of 8 decades, with the following conversion law:

$$V_{LOG} = 0.2 \log_{10}(I_{IN}/100pA) \quad (7.1)$$

Therefore the current is converted into a voltage range that can be directly acquired by an analog to digital converter (ADC).

The voltage across the input pin of the I-V converter is $V_1 = 0.5$ V and, as shown in Fig.7.6(a), the voltage across a sensing resistor is $(V_{DRIVE} + V_1) - V_1 = V_{DRIVE}$, therefore it is independent from V_1 . It is thus sufficient to change the value of V_{DRIVE} , fixed by a high precision voltage regulator, to adapt the range of the resistance variation (which depends on the constructional characteristics of the membranes) to the useful range of the I-V converter.

The output voltage of the I-V converter is sampled by a 12 bit analog to digital converter (ADC) embedded into the microcontroller, which also takes care of updating the channels of the multiplexer and serially sends the results to a PC. Each measurement is carried out at a frequency of 2 kHz so that, with a 8x8 matrix, the entire membrane is sampled at a frequency of about 30 Hz providing a true real time response and visualization.

7.2.2 Device calibration

In order to design the electronic read out circuit and to define the pressure/electrical resistance calibration curve, the investigated material was subjected to several compressive load/unload cycles. The output of the sensor and of the load cell of the MTS QTest/10 were simultaneously measured and compared. The calibration law was determined by fitting the voltage output signal of the sensor as function of the applied compressive pressure (Fig.7.7), obtaining:

$$P(kPa) = 310 \exp(1.1 * 10^{-3} S_{out}(mV)) \quad (7.2)$$

where P is the applied pressure and S_{out} is the output of the sensor.

In addition a homemade system was set up in order to investigate the response of the sensor to a variable position load and to control the cross talk effect between adjacent nodes

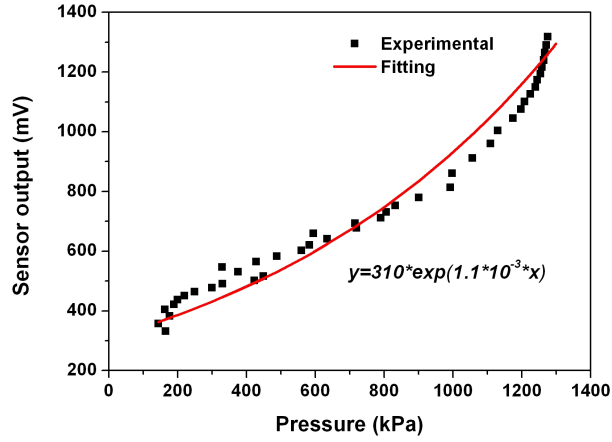


Figure 7.7. Experimental output of the sensor and fitting as function of applied uniaxial pressure

during a dynamic (translating) load.

A three axis motorized translation stage was employed to slither a tracer point (2.5 mm of tip radius) about on the sensor surface at different loads and velocities. The sensor was locked on the horizontal moving plate while the tracer point was fixed to the vertical Z axis. The scanning velocity was varied in the range 2.5-250 mm/s. The sensor was connected to the developed electronic circuit and example of the measured and saved data of variations of electrical tension are reported in Fig.7.8. The graphs of the Fig.7.8(b,c) show the signals collected during the test by the eight nodes of the second line at different scanning velocity. To verify the cross talk effect between adjacent nodes by adopting a safety approach, we applied a load that exceeds the maximum measurable pressure value in order to run the measurements with saturated signals (the curves plateau was reached at about 1500 mV). In this condition the presence of a cross talk phenomenon should be emphasized. The graph reported in Fig.7.8(d) shows the data of round trip measurement at slow velocity (2.5 mm/s) and by decreasing the pressure load during the measure. As expected the width of the saturated plateau progressively decreases and the curves assume a narrower peak shape. The different dynamic test performed with this apparatus showed a very slight amount of cross talk (signal time overlapping of two contiguous nodes), especially if we consider the relatively large size of the spherical tracer point (5 mm in diameter).

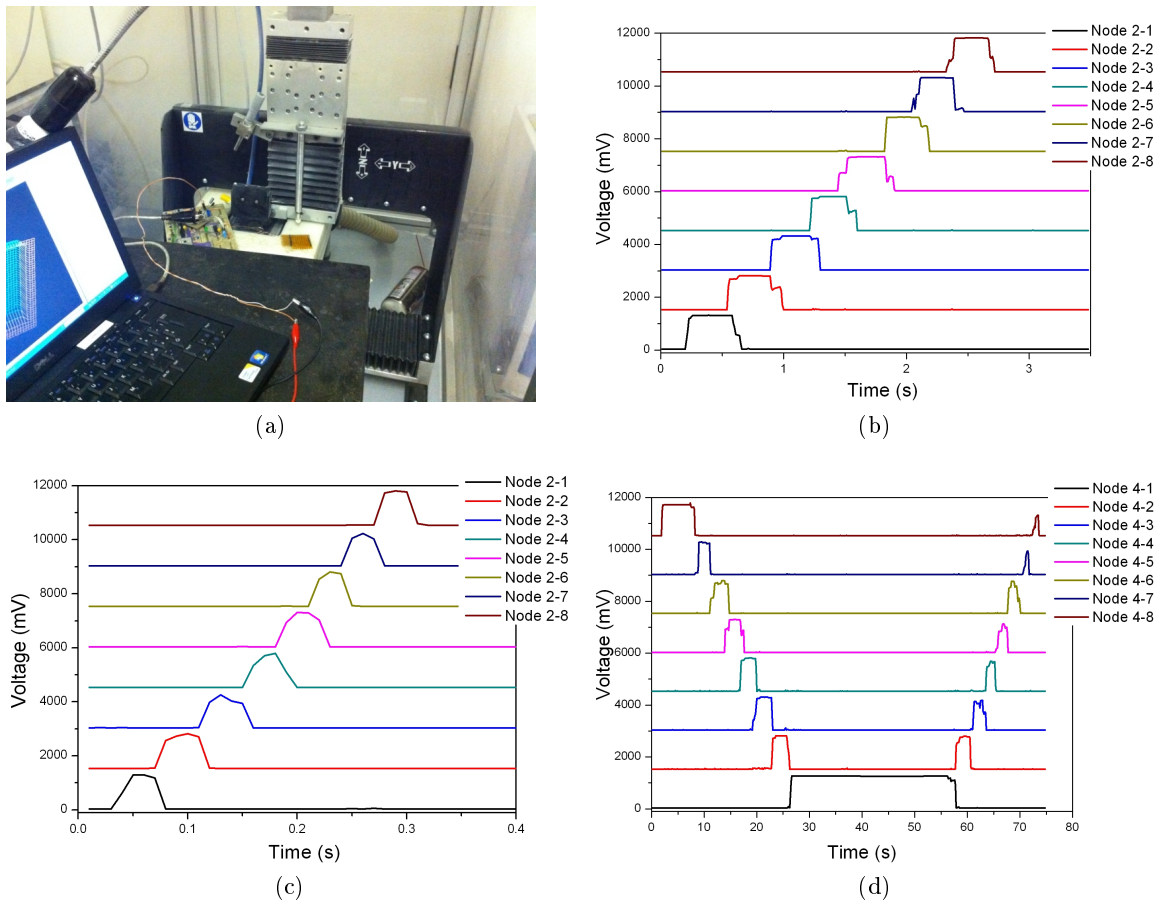


Figure 7.8. (a) Home-made apparatus for evaluating the sensor output signal on a line of the matrix and (b,c and d) sensor output voltage as function of time for different nodes of the matrix. Each node signal is translate up of 1500 mV for a better readability of the graph.

7.2.3 Sensor characterization

After the calibration, shown in Fig.7.7, the device was tested again with compressive load/unload cycles and the pressure output was compared to the one registered by the load cell of the MTS QTest/10. The result is shown in Fig.7.9. The output of the sensor is almost superimposed on the real applied pressure in the range from 300 up to 900 kPa, while a little discrepancy is present between 900 and 1150 kPa due to the saturation of the sensor output. Over 1150 kPa the sensor output is saturated and the measure is not anymore trustworthy.

In order to permit the real-time analysis of the applied pressure over the whole matrix sensor a specifically designed computer program has been prepared. The software is able

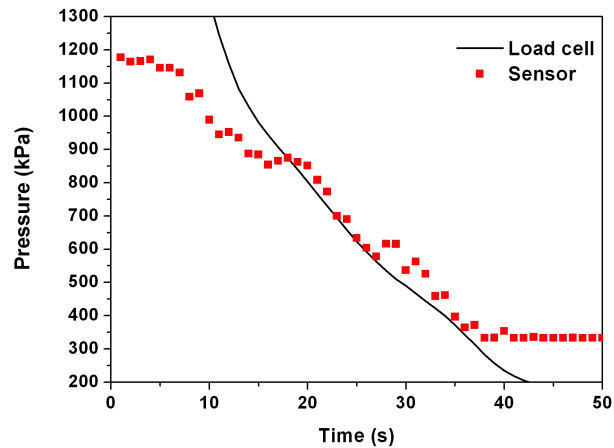


Figure 7.9. Comparison of the compressive pressure measured with the load cell of the MTS QTest/10 and with the piezoresistive sensor.

to receive and save the measurements of the 8×8 matrix, and to depict the distribution of the applied pressure in a 3D representation, highlighting the material deformation over the whole surface.

In Fig.7.10 are shown two pressure distributions measured with the piezoresistive sensor array. In the first picture the localized pressure was applied with a pen until saturation of the dynamics of the sensor. In contrast in the second case, it is shown the footprint of a hex key press with the fingers in two different points, that corresponds to the pixels measuring a pressure above 900 kPa.

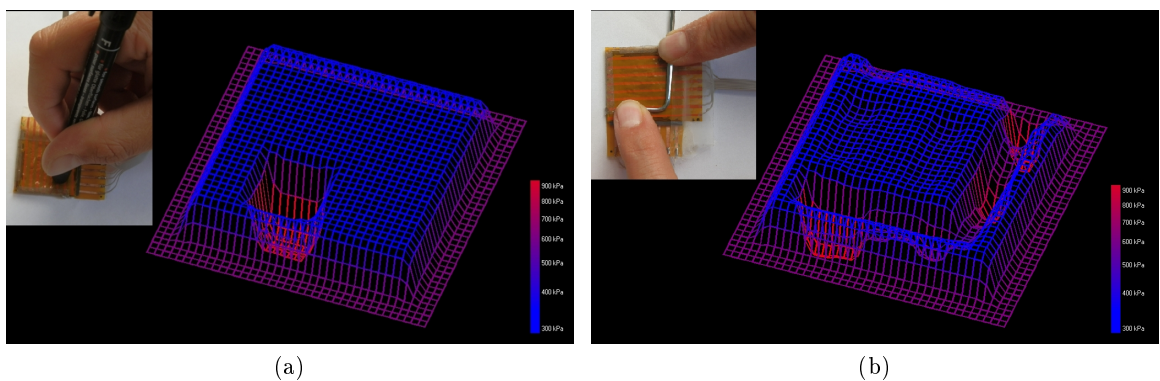


Figure 7.10. Pressure distribution measured with the piezoresistive sensor and visualized with the computer software. The load was applied with (a) a pen and (b) a hex key, as shown in the insets of the figures.

7.3 Second generation matrix tactile sensor

For the second version of the piezoresistive tactile sensor, the nickel particles were substituted with the copper ones as fillers for the functional composite for the reason already cited in chapter 6. Moreover the electrodes prepared with soft-lithography on copper metalized polyimide film were substituted with metallic strips directly deposited on the functional composite sheet.

The metal electrodes were deposited by the radio frequency magnetron sputtering technique on both the sample sides. Electrodes were patterned in the shape of 2 mm-wide parallel strips, eight on each side, in a way that they ideally perpendicularly crossed the the strips deposited on the opposite sample side, thus creating an 8x8 matrix of nodes (Fig.7.11). Each strip consisted of a first layer of titanium (~ 20 nm), working as adhesion layer, and a film of silver (~ 200 nm). The electrodes were characterized by a good adhesion to the surface of the composite, and preserved their conductivity even after several stretching and compressive deformations. Each electrode was connected to an equivalent pattern, fabricated on Cu-metalized polyimide, by means of a conductive silver paste. Finally the sensor was passivated with a few micrometers thick layer of pure PDMS (10:1 base-curing agent ratio by weight) by the spinning technique to protect the sensor composite material and the electrodes.

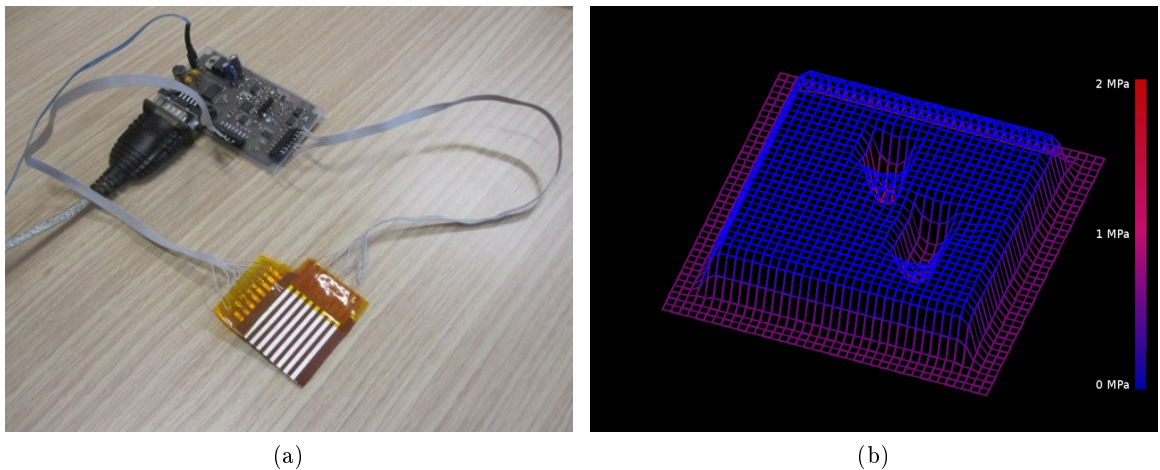


Figure 7.11. (a) Image of the sensor connected to the dedicated electronic board and (b) screenshot of the computer program during a measurement session.

A new version of the customized electronic circuit was fabricated on a printed circuit board (PCB) to monitor the resistance value of each node of the sensor matrix (Fig.7.11(a)). The main advantages of the PCB version of the circuit respect to the breadboard one are the shrinking of the dimensions and above all the noise reduction.

The sensor prepared with the PDMS-Cu composite was calibrated with the same procedure of the nickel based one and the software was update with the obtained conversion law. Since the variation of electrical resistance is lower with respect to the PDMS-Ni as shown in chapter 6, with the dynamic of the electric board is possible to measure applied pressure up to 2 MPa, but with a lower resolution. An example of a pressure distribution applied to the matrix sensor is shown in Fig.7.11(b) with a screenshot of the computer program during a measurement session.

Further measurements on resolution, x-y sensitivity and reproducibility are going on to provide an exhaustive characterization and knowledge of the new version of matrix tactile sensor.

Bibliography

- [1] Y. Huang, X. Zhao, Q. Yang, S. Wu, and C. Liu. Flexible tactile sensor system for robot skin based on LabVIEW. *2012 IEEE International Conference on Information and Automation, ICIA 2012*, pages 563–567, 2012.
- [2] M.H. Lee and H.R. Nicholls. Tactile sensing for mechatronics - A state of the art survey. *Mechatronics*, 9(1):1–31, 1999.
- [3] V.J. Lumelsky, M.S. Shur, and S. Wagner. Sensitive skin. *IEEE Sensors Journal*, 1(1):41–51, 2001.
- [4] H. Yousef, M. Boukallel, and K. Althoefer. Tactile sensing for dexterous in-hand manipulation in robotics - A review. *Sensors and Actuators, A: Physical*, 167(2):171–187, 2011. cited By (since 1996) 12.
- [5] S.Y. Fu, X.Q. Feng, B. Lauke, and Y.W. Mai. Effects of particle size, particle/matrix interface adhesion and particle loading on mechanical properties of particulate-polymer composites. *Composites Part B: Engineering*, 39(6):933–961, 2008.

- [6] R.S. Dahiya, G. Metta, M. Valle, and G. Sandini. Tactile Sensing-From Humans to Humanoids. *Robotics, IEEE Transactions on*, 26(1):1–20, 2010.
- [7] K. Kim, K.R. Lee, W.H. Kim, K.B. Park, T.H. Kim, J.S. Kim, and J.J. Pak. Polymer-based flexible tactile sensor up to 32 x 32 arrays integrated with interconnection terminals. *Sensors and Actuators, A: Physical*, 156(2):284–291, 2009.
- [8] J. Engel, J. Chen, and C. Liu. Development of polyimide flexible tactile sensor skin. *Journal of Micromechanics and Microengineering*, 13(3):359–366, 2003.
- [9] E.S. Hwang, J.H. Seo, and Y.J. Kim. A polymer-based flexible tactile sensor for both normal and shear load detections and its application for robotics. *Journal of Microelectromechanical Systems*, 16(3):556–563, 2007.
- [10] Harsaanyi G. Polymer films in sensor applications: a review of present uses and future possibilities. *Sensor Review*, 20(2):98–105, 2000.
- [11] M. Inaba, Y. Hoshino, K. Nagasaka, T. Ninomiya, S. Kagami, and H. Inoue. A full-body tactile sensor suit using electrically conductive fabric and strings. In *Intelligent Robots and Systems '96, IROS 96, Proceedings of the 1996 IEEE/RSJ International Conference on*, volume 2, pages 450–457 vol.2.
- [12] M.E.H. Eltaib and J.R. Hewit. Tactile sensing technology for minimal access surgery - a review. *Mechatronics*, 13:1163–1177, 2003.
- [13] C. Ricciardi, G. Canavese, R. Castagna, I. Ferrante, A. Ricci, S.L. Marasso, L. Napione, and F. Bussolino. Integration of microfluidic and cantilever technology for biosensing application in liquid environment. *Biosensors and Bioelectronics*, 26(4):1565–1570, 2010.
- [14] L. Gitlin, P. Schulze, and D. Belder. Rapid replication of master structures by double casting with PDMS. *Lab on a Chip - Miniaturisation for Chemistry and Biology*, 9(20):3000–3002, 2009.
- [15] S.C.B. Mannsfeld, B.C.-K. Tee, R.M. Stoltenberg, C.V.H.-H. Chen, S. Barman, B.V.O. Muir, A.N. Sokolov, C. Reese, and Z. Bao. Highly sensitive flexible pressure sensors with microstructured rubber dielectric layers. *Nature Materials*, 9(10):859–864, 2010.

- [16] D.J. Lipomi, M. Vosgueritchian, B.C.-K. Tee, S.L. Hellstrom, J.A. Lee, C.H. Fox, and Z. Bao. Skin-like pressure and strain sensors based on transparent elastic films of carbon nanotubes. *Nature Nanotechnology*, 6(12):788–792, 2011.

Chapter 8

A quasi-digital wireless system for piezoresistive composite sensors

The piezoresistive composites reported in the previous chapters vary not only their electrical resistance under the application of a pressure, but also their capacitance. Since the material basic unit consists of an insulating dielectric layer (the tunnelling barrier) between two metallic particles, it forms a capacitor. When deformed, the interparticle layer decreased, increasing the capacitance of the unit and consequently the one of the whole composite sample.

A new sensor architecture was designed to exploit both the resistance and the capacitance variation to measure pressure with a very high sensitivity and fast response. The signal is then wireless transmitted to the PC interface for elaboration by a IR-UWB (Impulse-radio Ultra-wide-band) transmitter. An implementation of a sensor network without wiring to be mounted onto robot hands and body has been studied and is under development. Anyway a first prototype sensing element has been fabricated, mounted and tested on ESA robotic assistant EUROBOT.

8.1 Sensor network architecture

A network of sensing elements for pressure detection in a humanoid robot was designed in order to increase the sensitivity, to obtain real time measurements and to reduce dimensions (implementing CMOS technology) wiring and power consumption.

Each sensing node consists of a sample of PDMS-Cu composited prepared between two

copper metalized polyimide film. The shape of the elements depends on the position they are allocated in the robot hand. The piezoresistive sensors are then connected to the read-out circuit able to manage up to 16 nodes, placed in the palm, as shown in Fig.8.1. A different approach was used to design the electronics. The classical architecture uses a single read-out circuit able to switch and manage an array of sensing elements (as for the sensor array presented in the previous chapter) [1, 2]. While in our approach, the integrated circuit (IC) includes many circuit replicas with very small size and low-power consumption each, allowing parallel signal acquisition [3].

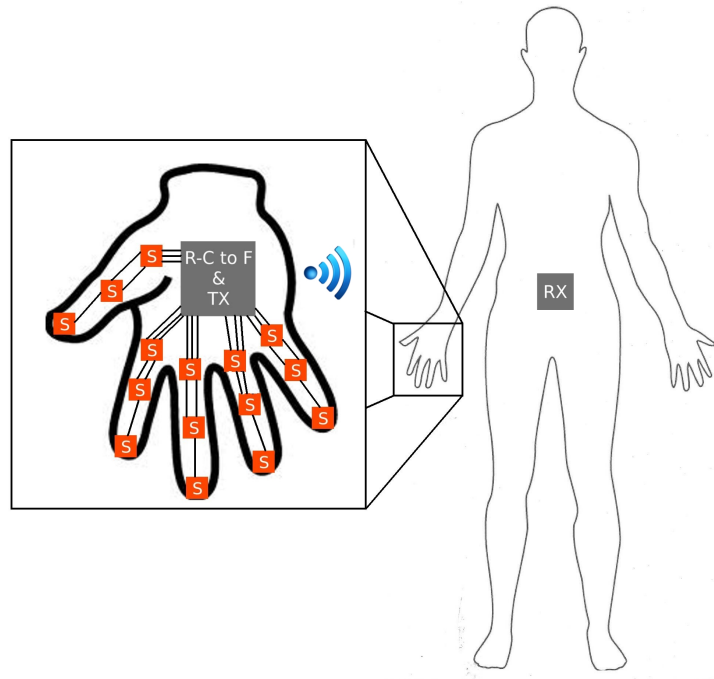


Figure 8.1. Schematic of the sensor architecture integrated on a humanoid robot

The read out circuit exploits a quasi-digital solution, converting resistance (R) and capacitance (C) values of the sensor in to a frequency signal. The signal is then wireless transmitted with a Impulse-radio Ultra-wide-band transmitter to a receiver placed on the robot body where all the signal will be processed because of a easier power availability. The quasi-digital signal is compatible with the IR-UWB circuit and can be transmitted without any further elaboration, reducing transmission time and power. From the receiver the signal

is then elaborated by a PC interface that converts the frequency in pressure values.

8.1.1 R,C-to-F converter

A direct resistance measurement can be possible, converting resistance variation into analog voltage signal. Such output value usually needs to be converted into digital signal of N-bits, for being used by digital units for signal processing (DSP). Even in an array structure of several sensing elements, it is suitable to manage digital values. Thus, the A/D conversion circuit has to be included into each sensing element for allowing parallel data acquisition in the array. In that sense, the complexity of the array architecture dramatically increases.

Our purpose is to limit the complexity of the whole system in order to reduce power consumption and silicon area. A conventional solution to directly convert resistance and capacitance value into a digital signal regards the use of a relaxation oscillator whose resonating frequency is determined by the resistance and capacitance under measurement [4]. The R,C-to-F converter has a 1-bit quasi-digital output with an oscillation period that is an analog conversion of the resistance and capacitive variations. Quasi-digital techniques have been also proposed as an extension of IEEE standard sensor interface [5]: these enable significant advantages especially when the sensors need to be placed in a harsh environment or when the measured signal needs to be transmitted over a long distance [6]. An analog output in fact could be perturbed by noise due to interference or coupling effects. Moreover, a 1-bit quasi-digital signal can be easily managed in an array architecture.

An external unit (e.g. programmable DSP or μ Controller), where strict constraints for power and area are not imposed, will be in charge of converting the quasi-digital signal to an N-bit representation for digital signal processing [7]. Moreover, a quasi-digital signal can be directly interfaced to an asynchronous IR-UWB transmitter [8] for wireless data transmission, since the compatibility of the signal.

The standard RC oscillator, based on Schmitt Trigger (ST) architecture, has low power consumption and low complexity, but standard circuits do not achieve high oscillation frequency for our resistive and capacitive range of our interest. When used in real-time applications, a quasi digital sensor would require high reactivity: the back-end computation time required for the detection of an event shall be small compared to the time-constant of the physical quantity under measurement. Hence, frequency shall be kept as high as possible to allow a fast reaction to dynamic resistance variations, both for characterization and raw on/off digital decisions.

To increase oscillation frequency compared to standard ST-based RC oscillators, we propose a circuit with very narrow equivalent hysteresis gap [9]. The circuit comprises a standard ST and an operational amplifier (OpAmp) connected to the same output terminal. Oscillation frequency is defined by the equivalent resistance and capacitance of the sensor and the amplifier AC characteristics.

We define this hybrid circuit as “Operational Schmitt Trigger” (OST), since it integrates the bistable properties of a ST and the AC response of an OpAmp. The R,C-to-F converter occupies $\sim 0.005 \text{ mm}^2$ silicon area and has a simulated power consumption of $142 \mu\text{W}$ at 1.2 V supply.

8.1.2 IC-UWB transmitter

A very low-complexity all-digital IR-UWB transmitter able to generate pulses in the band 0-5 GHz, was implemented for the wireless transmission of the quasi-digital signal [8]. The transmitter, that requires a silicon area lower than a PAD for signal I/O is prototyped in a 130 nm RFCMOS technology and includes analog control signals for frequency and bandwidth tuning. Center frequency is linearly selected with voltage supply, 0.5 V for the range 0-960 MHz and 1.1 V supply for the higher 3.1-5 GHz range. The architecture is based on the same delay cell for both baseband and radio frequency signal generation, and pulses fractional bandwidth remains constant when voltage supply and control voltages scale. At 420 MHz center frequency, the transmitter achieves 7 pJ/pulse, and for 4 GHz center frequency pulses, it achieves 32 pJ/pulse active energy consumption. The OOK/S-OOK (on/off keying, synchronized-on/off keying) transmitter occupies an area of 0.004 mm^2 . For amplitude shift keying (ASK) modulation, the system includes a separate on-chip capacitor bank connected to the output of the transmitter for an overall size of 0.024 mm^2 .

For our application the signal are transmitted at a center frequency of 3.3 GHz with a bandwidth of 500 MHz. The energy consumption per event transmitted is around 30 pJ, a very low value for sensor application.

8.2 Prototype fabrication

The sensor network fabrication is under development at this moment, since the silicon chip including 16 R,C-to-F converter circuits has not been fabricated yet.

The proof of concept of this whole architecture has been demonstrated by using a single

sensor with a single converter. The quasi-digital signal was then wireless transmitted with the IC-UWB transmitter to the board with the receiver connected to the PC. A schematic of the system architecture is reported in Fig.8.2. A program, developed with Processing software, acquires the data and computes the average value and standard deviation from over 100 measures every second. Calibration process has still to be performed in order to convert the frequency in pressure values directly by software.

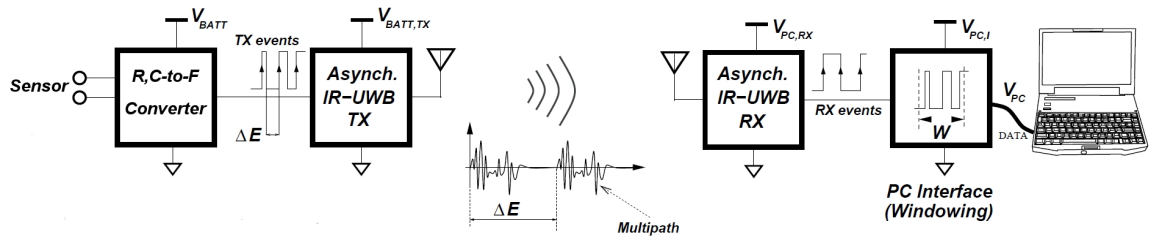


Figure 8.2. System-level architecture of the whole sensor device.

Static pressure measurements were performed on the piezoresistive sensor element by applying different loads. Thanks to this measurement system was possible to resolved 1 gr of applied load, as reported in Fig.8.3 and in Tab.8.1. The system is very sensible for small load, while tends to saturate for higher ones (over 1500 gr). This behaviour is more appreciable in the linear plot of Fig.8.3(a). Samples with different area ($10 \times 10 \text{ mm}^2$ and $20 \times 20 \text{ mm}^2$) were tested, showing different variation of the resonant oscillation frequency.

The sensor was then mounted on the hand of the robotic assistant EUROBOT (Fig.8.4) fabricated by Thales Alenia for ESA (European Space Agency) for demonstrating its possible application in robotic device [10]. The sensor was able to detect the pressure applied by the robot while grasping both an iron bar and a piece of foam rubber, as shown in Fig.8.5(a), in real time. The measured frequency oscillation was wireless transmitted, and plotted and visualized on a PC (Fig.8.5(b)).

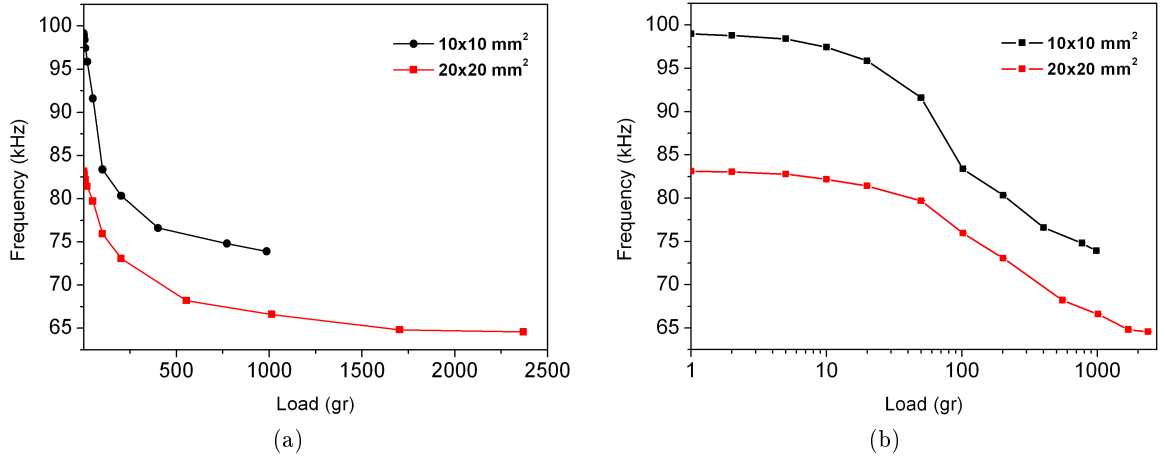


Figure 8.3. Resonant oscillation frequency as function of the applied static load plotted in (a) linear and (b) logarithmic scale for 2 different sensors.

20x20 mm ² sensor			10x10 mm ² sensor		
Load (gr)	Frequency (Hz)	σ (Hz)	Load (gr)	Frequency (Hz)	σ (Hz)
0	83170	18	0	99160	18
1	83100	17	1	98970	15
2	83040	17	2	98780	15
5	82780	20	5	98400	14
10	82180	18	10	97440	17
20	81400	16	20	95860	22
50	79700	18	50	91600	24
102	75940	20	102	83366	23
202	73060	19	202	80340	22
554	68210	17	401	76600	17
1014	66600	16	772	74800	16
1703	64810	15	986	73900	19
2370	64570	16			

Table 8.1. Resonant oscillation frequency and standard deviation as function of the applied static load for 2 different sensors.

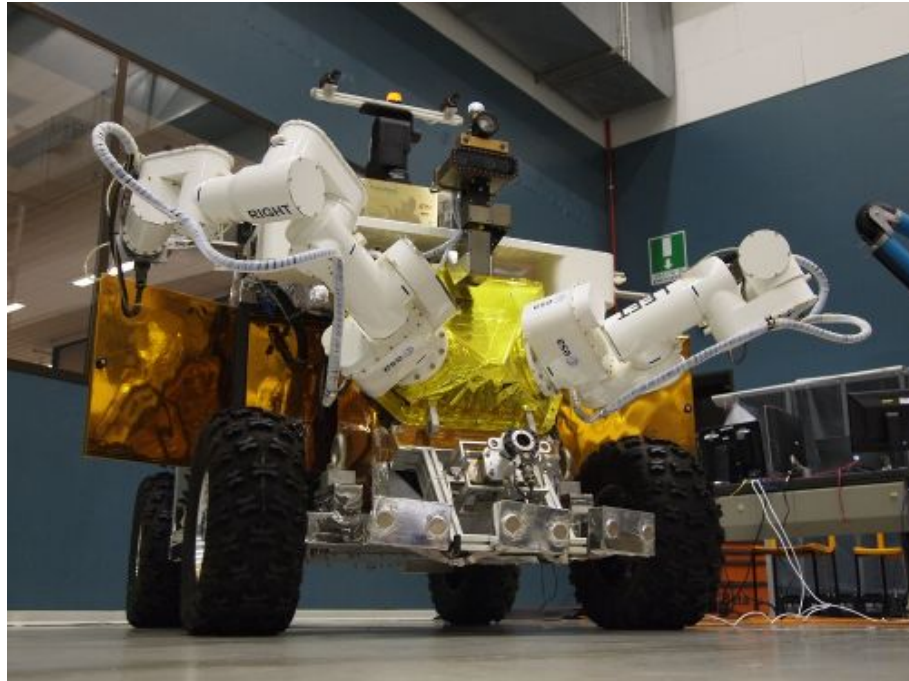


Figure 8.4. Image of EUROBOT.

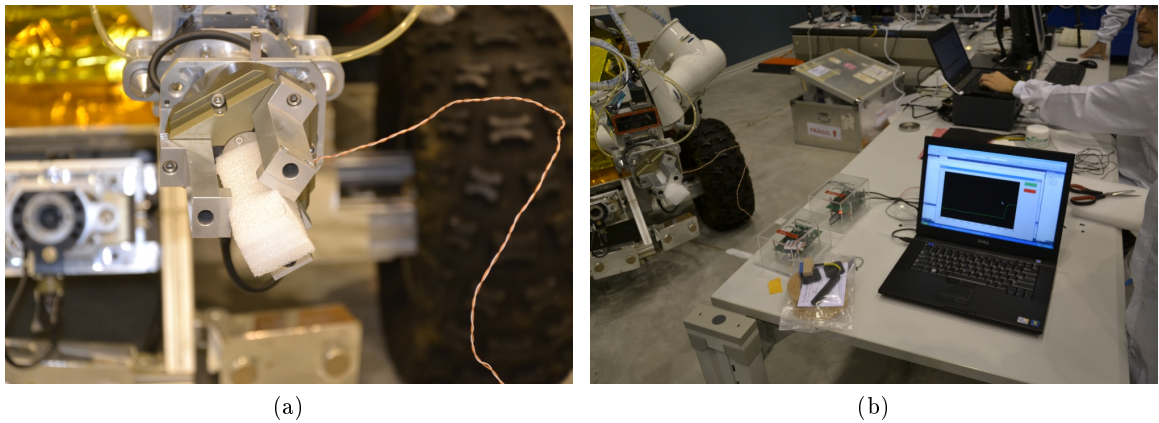


Figure 8.5. Images of EUROBOT grasping a piece of foam rubber with integrated the developed tactile sensor measuring the applied pressure.

Bibliography

- [1] H. Liu, T.H. Teo, and Y.P. Zhang. A Low-power Wide-range Interface Circuit for Nanowire Sensor Array Based on Resistance-to-Frequency Conversion Technique. In

- IEEE International Symposium on Integrated Circuits*, pages 13–16, 2009.
- [2] F. Conso, M. Grassi, P. Malcovati, and A. Baschiroto. A Very High Dynamic Range Interface Circuit for Resistive Gas Sensor Matrix Read-out. In *IEEE International Symposium on Circuits and Systems*, pages 2209–2212, 2011.
- [3] K. Lasanen and J. Kostamovaara. A 1.2-V CMOS *RC* Oscillator for Capacitive and Resistive Sensor Applications. *IEEE Transactions on Instrumentation and Measurement*, 57(12):2792–2800, 2008.
- [4] K. Mochizuki and K. Watanabe. A high-resolution, linear resistance-to-frequency converter. *IEEE Transactions on Instrumentation and Measurement*, 45(3):761–764, 1996.
- [5] S.Y. Yurish. Extension of IEEE 1451 Standard to Quasi-Digital Sensors. In *IEEE Sensors Applications Symposium*, pages 1–6, 2007.
- [6] S.Y. Yurish. Low-cost, smart temperature sensors systems based on Universal Frequency-to-Digital Converter. In *IEEE Sensors Applications Symposium*, pages 287–292, 2009.
- [7] C. Azcona, B. Calvo, N. Medrano, A. Bayo, and S. Celma. 12-b Enhanced Input Range On-Chip Quasi-Digital Converter With Temperature Compensation. *IEEE Transactions on Circuits and Systems II: Express Briefs*, 58(3):164–168, 2011.
- [8] M. Crepaldi, D. Daprà, A. Bonanno, I. Aulika, D. Demarchi, and P. Civera. A Very Low-Complexity 0.3–4.4 GHz 0.004 mm² All-Digital Ultra-Wide Band Pulsed Transmitter for Energy Detection Receivers. *IEEE Transactions on Circuits and Systems–I*, PP(99):1–13, 2012.
- [9] A. Bonanno, M. Crepaldi, I. Rattalino, P. Motto, D. Demarchi, and P. Civera. A 0.13 μm CMOS Operational Schmitt Trigger R-to-F Converter for Nanogap-based Nanosensors Read-out. *IEEE Transactions on Circuits and Systems–I*, In press.
- [10] http://www.esa.int/esaHS/SEM9NCZGRMG_research_0.html.

Conclusion

The thesis reports on the preparation of three piezoresistive composites using different commercial metal particles as filler in a silicone (PDMS) matrix. The results obtained from the functional characterizations performed under compressive and tensile stresses are well supported by the theoretical models and showed that the conduction mechanism in the metal-polymer composite is based on a quantum tunnelling effect. The phenomenon is further enhanced by the sharp tip morphology of the metal particles used. In particular when using spiky nickel particles, the composites undergo to a variation of resistance up to nine orders of magnitude under an applied pressure. The possibility to obtain a huge variation in resistance upon a small deformation of the samples makes this composite a well performing functional material for sensor applications. Moreover the simplicity of the synthesis process, the low cost of the materials and the mechanical flexibility favor its choice among the possible sensing materials for tactile sensors. Similarly, piezoresistive composites based on spiky copper particles and ad-hoc synthesized gold nano-stars were also prepared and characterized. A comparison of the three materials is also reported.

Piezoresistive composites were subsequently implemented in two different sensor architectures. The first measures the resistance variation of a 8x8 array of sensing element and reproduces the pressure distribution on a 3D graphic software. The second exploits both the resistance and capacitance variation of the tunnelling conductive material with an extremely low power quasi-digital frequency converter methods. Thanks to this measuring methods, the sensor was able to resolve 1 gr of applied load. Further work will implement the device in a sensor network with wireless transmission for reducing power and wiring. The network will be suitable for the application on the hands of a humanoid robot, as already demonstrated on the robot assistant EUROBOT.

List of Publications

- [1] S. Stassi, G. Canavese, F. Cosiansi, R. Gazia, and M. Cocuzza. A Tactile Sensor Device Exploiting the Tunable Sensitivity of Copper-PDMS Piezoresistive Composite. *Procedia Engineering*, 47:659–663, 2012.
- [2] S. Stassi and G. Canavese. Spiky nanostructured metal particles as filler of polymeric composites showing tunable electrical conductivity. *Journal of Polymer Science, Part B: Polymer Physics*, 50(14):984–992, 2012.
- [3] F. Cosiansi M. Cocuzza S. Stassi, G. Canavese. An innovative copper-PDMS piezoresistive composite for flexible tactile sensor. In *Proceeding of the 15th European Conference on Composite Materials, Venice (Italy)*, 2012.
- [4] S. Stassi, G. Canavese, V. Cauda, S.L. Marasso, and C.F. Pirri. Evaluation of different conductive nanostructured particles as filler in smart piezoresistive composites. *Nanoscale Research Letters*, 7, 2012.
- [5] S. Stassi, V. Cauda, G. Canavese, D. Manfredi, and C.F. Pirri. Synthesis and characterization of gold nanostars as filler of tunneling conductive polymer composites. *European Journal of Inorganic Chemistry*, 16:2669–2673, 2012.
- [6] G. Canavese, S. Stassi, M. Stralla, C. Bignardi, and C.F. Pirri. Stretchable and conformable metal-polymer piezoresistive hybrid system. *Sensors and Actuators, A: Physical*, 186:191–197, 2012.
- [7] G. Canavese, M. Lombardi, S. Stassi, and C. F. Pirri. Comprehensive characterization of

large piezoresistive variation of Ni-PDMS composites. *Applied Mechanics and Materials*, 110-116:1336–1344, 2012.

- [8] S. Stassi, G. Canavese, M. Lombardi, A. Guerriero, and C.F. Pirri. Giant piezoresistive variation of metal particles dispersed in PDMS matrix. *MRS Online Proceedings Library*, 1299, 2011.